Journal of the European Ceramic Society 21 (2001) 2161–2170

www.elsevier.com/locate/jeurceramsoc

Sub-scalar reactions during oxidation of I_w-phase SiAlON glass–ceramics under a very low oxygen partial pressure

Ian MacLaren [a,*], Lena K.L. Falk [a], Aranzazu Díaz [b], Stuart Hampshire [b]

[a] *Department of Experimental Physics, Chalmers University of Technology, SE-412 96 Göteborg, Sweden*
[b] *Materials and Surface Science Institute, Ceramics Research Unit, University of Limerick, Limerick, Ireland*

Received 29 June 2000; received in revised form 21 December 2000; accepted 12 January 2001

Abstract

YSiAlON I_w glass–ceramic microstructures affected by surface oxidation during crystallisation have been compared with bulk microstructures which were unaffected by oxidation using transmission electron microscopy. The sub-scalar microstructures were found to have anomalously large I_w crystals (around twice the size of those in the unaffected bulk material), and some large γ and δ phase $Y_2Si_2O_7$ crystals were also present. Compositional analysis using EDX and EELS showed that the composition of the I_w crystals was independent of their location below the oxidised surface, and that the N content of the I_w phase was significantly lower than previously believed, around 2 anion%. The residual glass composition in the sub-scalar volumes was more strongly affected by the diffusion processes occurring during oxidation, but in an inhomogeneous way. Areas mostly surrounded by I_w grains were little affected and showed little deviation of the N content from the average value for unaffected bulk residual glass of around 8 anion%. More open areas of sub-scalar glass, however, showed noticeably reduced N contents of less than 5 anion% N, and in some cases also an enrichment in Y. It was concluded that oxidation in the subscalar region is initiated mainly through diffusion in the more open areas of glass associated with an inward diffusion of O and the diffusion of cations leading to the local formation of $Y_2Si_2O_7$ crystals.

Keywords: Diffusion; Electron microscopy; Glass–ceramics; Oxidation; Sialon

1. Introduction

One of the fundamental restrictions on the use of Si_3N_4 and SiAlON based ceramics is the tendency for these materials to undergo oxidation at elevated temperatures. The oxidation of MSiAlON glasses and glass–ceramics has been investigated in several studies.[1–5] It has been clearly shown using scanning electron microscopy (SEM) that a surface scale is produced, which tends to be crystalline with some porosity due to the formation of nitrogen bubbles.[1,3,4] Also, a mismatch in mechanical properties between the scale and the bulk MSiAlON tends to result in cracking of the scale at the specimen corners on long term oxidation.[3,4] The relative effects of different oxidising atmospheres including partial pressures of oxygen and water vapour have been studied.[1,3–5] Reaction rate analysis has also been applied to the determination of the reaction mechanisms proceeding during oxidation and it was concluded that the limiting step in the oxidation process, i.e. the progress of the internal interface between the scale and the bulk, is reaction controlled.[3–5] This is in contrast to the situation in Si_3N_4 and β-SiAlON ceramics, where it has generally been concluded that the oxidation is diffusion controlled, governed by the diffusion of oxygen and other ionic species through the intergranular glassy phase.[6–9]

Whilst some information is known about the formation and structure of oxide scales on SiAlON glasses and glass–ceramics.[1,3–5] very little is known of the microstructural changes happening in the sub-scalar region during oxidation. To perform more detailed microstructural characterisation of oxide scales and sub-scalar regions on these glass-ceramics using transmission electron microscopy (TEM) is difficult due to the high porosity and the fragile nature of these scales. Recent work has been performed, however, on the characterisation of

* Corresponding author at Max Planck Institut für Metallforschung, Seestr. 92, 70174 Stuttgart, Germany.
E-mail address: ian.maclaren@physics.org (I. MacLaren).

0955-2219/01/$ - see front matter
PII: S0955-2219(01)00192-3

the oxide scale and sub-scalar regions on a rare earth B-phase (Y_2SiAlO_5N) MSiAlON glass–ceramic.[10]

The I_w phase is a MSiAlON phase which can be formed for M = Y, Er,[11] and is closely related to the B-phase.[12] It is, in fact, an ordered version of the hexagonal B-phase[13] having a monoclinic structure[14] and a ratio of cations, M:Si:Al around 3:2:1 or 5:3:2.[11,15,16] The nitrogen content has not previously been determined directly for this phase. Recent work has shown that I_w glass–ceramics containing 20–40% residual glass and sub-micron I_w crystals can be formed from Y- or Er-SiAlON compositions.[11] The residual glass content was found to be dependent on the cation starting composition (for a constant N/O ratio) and independent of crystallisation temperature in the range 1100–1150°C, with starting M:Si:Al ratios of 3.45:3:2 and 3:3:2 giving a glass contents of about 20–25% and about 35%, respectively. Crystal size is little affected by starting composition, however, and is mainly dependent on crystallisation temperature.[11] It appears that crystals mainly grow by coalescence[11], a process that results in the formation of orientational domain boundaries.[17]

In this present study, attention is focussed on the microstructural and chemical processes occurring in the sub-scalar region as a result of surface oxidation of the residual glass in I_w-phase Y–Si–Al–O–N glass–ceramics during crystallisation heat-treatment under a very low partial pressure of oxygen and/or water vapour.

2. Experimental procedure

I_w-phase Y–Si–Al–O–N glass–ceramics were prepared as described previously.[11] Y_2O_3, Si_3N_4, SiO_2 and Al_2O_3 powders were mixed, cold isostatically pressed, and melted at 1715°C under flowing N_2 for 1 h (N_2 purity > 99.997%, O < 15 ppm, H_2O 1–4 ppm, flow rate 70 cm^3 min^{-1}). The melt was then removed from the furnace, rapidly poured into a graphite mould to yield a glass and annealed at 850°C for 1 h to remove stresses. Two different starting compositions were used, corresponding to Y:Si:Al = 3:3:2, and 3.45:3:2, both with the same N content of 10 eq.%.[11]

Glass pieces, of similar size and shape, crystallised at 1100 and 1200°C for 10 hours under a N_2 atmosphere (as specified above), to minimise oxidation, were included in the present study. It has previously been noted,[11,18] that heat-treatments of Y or RE SiAlONs may result in the formation of a thin oxidised layer on the surface of the material, even when the glass specimens are heat-treated under high purity nitrogen. This may be related to the presence of small amounts of residual air or water in the crystallisation furnace, or to the low partial pressure of oxygen (≈1.5 Pa) in the nitrogen gas used in the crystallisation heat-treatment. The crystallised glass–ceramic specimens in the present study had a thin oxidised layer at the surface, which could be clearly identified as it had a lighter grey coloration than the bulk material.

Samples for SEM were prepared by cutting through the crystallised glass–ceramic with a diamond saw and mounting one of the pieces in epoxy resin. The cross-sections were then polished using diamond pastes down to a 1 μm diamond finish. These were then gold sputter-coated and examined using a Jeol JSM-840 SEM in backscattered electron detection mode using an accelerating voltage of 20 kV.

Two pairs of specimens were prepared for TEM, see Table 1. In order to provide comparisons between the sub-scalar microstructure affected by the surface oxidation and the unaffected glass-ceramic microstructure, one pair of specimens was taken from the sub-scalar and central regions of the 3:3:2 glass crystallised at 1100°C. The other pair of specimens was taken from the centre of the 3:3:2 and 3.45:3:2 specimens crystallised at 1200°C. The crystalline phase assemblage of the regions studied in the TEM is listed in Table 1, determined using both XRD and TEM where possible (the sub-scalar region could only be studied by TEM).

Slices for thin foil preparation were cut using a diamond saw and these were then polished on both sides to a thickness of ≈100 μm, 3 mm discs were cut using an ultrasonic disc cutter, and the discs were then dimpled such that the central region had a thickness of 30 μm. The samples were then thinned to perforation using ion beam milling (Gatan PIPS) at 5 kV and an angle of ±8–10°, with final thinning at a lower angle of ≈6° and 3 kV to minimise ion beam damage in the thin area. Finally, the samples were coated with a thin film of carbon (nominal thickness 4 nm) to prevent charging in the TEM.

TEM characterisation was performed using a Philips CM200 FEG (accelerating voltage 200 kV) equipped with an Oxford Instruments Link ISIS EDX system and a Gatan Imaging Filter (GIF). Techniques used included bright field imaging, selected area diffraction, EDX analysis (for determination of cation composition), and EELS using the GIF (for determination of anion composition from the N:O ratio).

Identification of electron diffraction patterns was performed using the auto-indexing function of the EMS On line software,[19] as described previously.[20]

Table 1
Details of the experimental materials

Y:Si:Al	Cyrstallisation	Location of TEM thin foil	Crystalline phase composition (by XRD and/or TEM)
3:3:2	1100°C/10 h	Sub-scale	I_w, γ-$Y_2Si_2O_7$, δ-$Y_2Si_2O_7$
3:3:2	1100°C/10 h	Specimen centre	I_w
3:3:2	1200°C/10 h	Specimen centre	I_w, δ-$Y_2Si_2O_7$, others with low intensity peaks
3.45:3:2	1200°C/10 h	Specimen centre	I_w

The following methodology was used in the collection and quantification of EEL spectra. Spectra were collected in diffraction mode to ensure that the area of analysis was well defined. A value of the beam convergence was set by appropriate choice of condenser aperture to ensure that the convergence semiangle, α, was less than the entrance semiangle for the GIF, β, since this eliminates the need for a convergence angle correction.[21] A dispersion of 0.3 eV/channel was used in this work, as this gave a fair spectrum resolution of the zero loss peak and the edges, together with a large enough range of energies to record both the N K (401 eV) and O K (532 eV) edges, together with sufficient background below the N K edge and above the O K edge, all on the same spectrum. Moreover, only very thin areas were used for the collection of EEL spectra to eliminate any need for correction for the effects of multiple scattering. Firstly, a low loss spectrum was recorded and the beam spread again immediately after collection, to ensure that no more beam damage could be done to the area than absolutely necessary. The low-loss spectrum was then quantified to determine the thickness using the Gatan EL/P software, and as long as the thickness was under 0.15 λ (where λ is the mean free path for inelastic scattering) the area could then be used for determination of the N:O ratio without need to correct for the effects of multiple scattering.[22] A second spectrum was then recorded with a drift tube offset of 350 eV and a longer acquisition time (usually 5 s). The N:O ratio was then determined from the EEL spectra using the Gatan EL/P software with Hartree–Slater cross-sections, an integration interval with an offset of -5 eV and a width of 55 eV, and a background offset of 40 eV and a width of 25 eV.

3. Microstructural and chemical characterisation

Fig. 1 shows a SEM image of a cross-section through the surface region of the 3:3:2 I_w material crystallised at 1100°C. This picture clearly shows the porous surface layer (A) that is already known to exist on the surface of oxidised SiAlONs, as well as a dense second layer (B) with many large, elongated crystals, the size of which tends to decrease with depth below surface. Below B there is a coarser, sub-scalar microstructure (C), which is of particular interest for this study, and will be compared with the fine grained structure in the central region of the glass-ceramic (D), well away from the oxidised surface. The central region of the specimen (D) has such a fine-grained structure that very little detail can be resolved in this SEM image, and has been characterised extensively in other studies.[11,17] XRD showed that the oxidised surface layers of such YSiAlON specimens consist of several phases including I_w, β-$Y_2Si_2O_7$, γ-$Y_2Si_2O_7$, and a small amount of aluminium silicate ($Al_2Si_4O_{10}$), while I_w was the only crystalline phase in the central part, see Table 1.

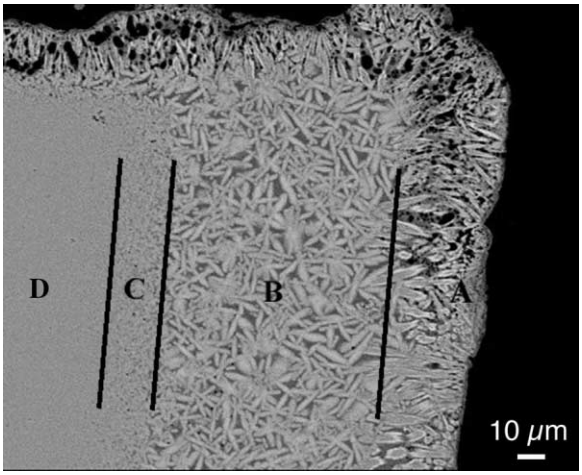

Fig. 1. Backscattered SEM image of a cross-section through the surface region of the 3:3:2 I_w material crystallised at 1100°C. The two layers of the surface scale are clearly visible (A and B), as is the coarse sub-scalar microstructure (C). The microstructure in the centre of the piece (D) is too fine to be resolved well by SEM.

The central part of the 3.45:3:2 specimen crystallised at 1200°C contained only I_w in addition to residual glass. XRD of the 3:3:2 specimen crystallised at 1200°C showed, however, the penetration of oxide phases (yttrium silicates and yttrium aluminium garnet) throughout the I_w glass-ceramic microstructure,[6] see Table 1.

Two microstructural features are clearly visible in TEM examination of the subscalar region of the 3:3:2 specimen crystallised at 1100°C. Firstly, the size of the I_w crystals in the glass-ceramic sub-scalar microstructure is anomalously large, as compared to the thin foil taken from the centre of the crystallised specimen. Secondly, there are also some large crystals of yttrium silicates present, in addition to the "normal" glass–ceramic microstructure that has previously been observed in these materials.[6] These two features will be discussed in turn and related to the bulk microstructures of the specimens crystallised at 1200°C, followed by compositional analysis of the phases involved. It should be pointed out that the microstructures characterised in the TEM were all fully dense.

3.1. Anomalously large I_w crystals

Fig. 2(a) and (b) show bright field TEM images of I_w crystals and glass in typical regions of the microstructure for the sub-scale and central regions, respectively, of the 3:3:2 specimen crystallised at 1100°C. It is clear that the grain size in the sub-scale sample is much larger. In addition to this, the large crystals of Fig. 2(a) show clear evidence of crystalline defects, which may well include rotational domain boundaries, as previously observed in larger I_w crystals.[17] Such large, faulted crystals are typically found in this sub-scalar region, and would be consistent with their having been formed by a coalescence process.[11,17]

The glass content in both the sub-scalar and bulk materials was estimated from dark field images taken using the objective aperture to select part of the diffuse diffraction ring for the amorphous glass as described elsewhere.[11] The glass content for the bulk has already been reported as $33\pm3\%$.[11] and the glass content for the sub-scalar material was found to be $35\pm5\%$. This shows clearly that the large crystal size in the sub-scalar region could not have been formed by increased crystallisation but only by coalescence of I_w crystals.

In a similar manner, a noticeable difference was found between the I_w crystal sizes in the bulk for the 3:3:2 and 3.45:3:2 specimens that had been crystallised at 1200°C for 10 h. As noted above, previous XRD results have shown that the 3:3:2 material suffered from a complete penetration of oxide phases throughout the bulk, whereas the 3.45:3:2 material still had the I_w glass-ceramic microstructure in the bulk.[11] TEM examination of the 3:3:2 material showed that it still contained large areas of I_w and glass, but that the crystal size in these areas was unusually large with crystal dimensions up to 1 μm: a low magnification bright field image of one area is shown in Fig. 3(a). In contrast to this, the I_w crystals of the 3.45:3:2 material were significantly smaller, although still larger than those in specimens crystallised at lower temperatures; an image of one area of this material is shown in Fig. 3(b) (both images in Fig. 3 were recorded at the same magnification). Thus, the I_w crystals in the oxidation-affected microstructures were much larger than in the microstructures that were, at least for the most part, unaffected by the oxidation. In both cases, the I_w crystals were quite faulted, although the faulting is perhaps more apparent in the larger crystals of the 3:3:2 material.

3.2. Large silicate crystals

Despite that one of the thin foils from the sample crystallised at 1100°C for 10 h was believed to come mainly from the sub-scale region (C in Fig. 1), it still contained some large (5–10 μm) yttrium disilicate ($Y_2Si_2O_7$) crystals,

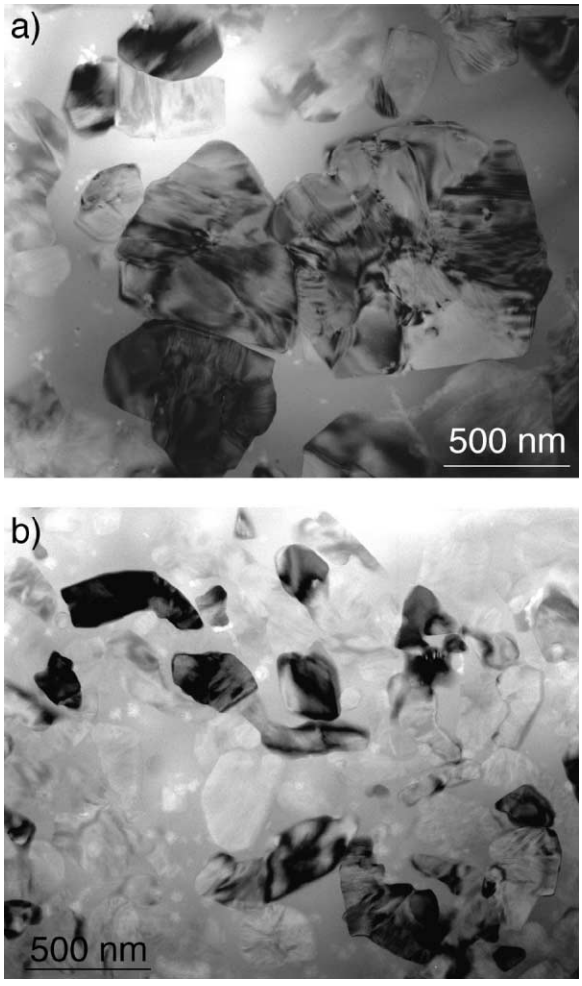

Fig. 2. Bright field TEM images of I_w crystals and glass in typical regions of the microstructure of the 3:3:2 specimen heat-treated at 1100°C for: (a) the sub-scale, and b) the central regions, respectively. A clear difference in I_w crystal size may be noted.

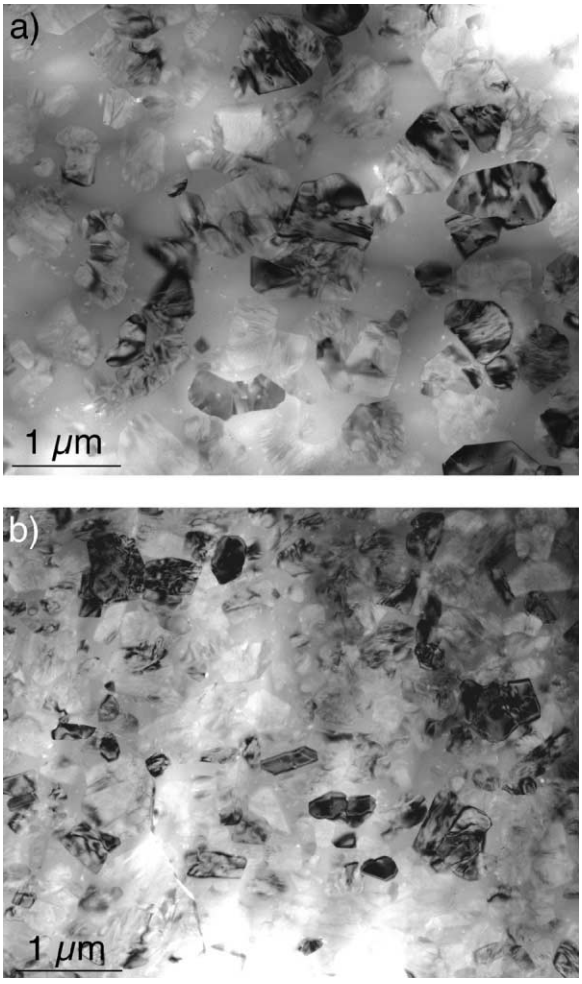

Fig. 3. Bright field TEM images of the I_w glass ceramic microstructure in a) the 3:3:2 material heat-treated at 1200°C, and (b) the 3.45:3:2 material heat-treated at 1200°C.

although most of the microstructure consisted of I_w crystals and glass. Fig. 4(a) shows some larger crystals that were shown by EDX to have a composition close to 50 cation% yttrium and 50 cation% silicon and to contain a significant amount of oxygen, although the amount was not quantified. These crystals are, thus, almost certainly $Y_2Si_2O_7$. These crystals all had the same crystallographic orientation and were probably all joined as one larger crystal prior to thinning. It may also be noted that there are comparatively large areas of glass separating adjacent $Y_2Si_2O_7$ crystals [Fig. 4(a)].

Fig. 4(b) and (c) shows two selected area diffraction (SAD) patterns obtained from one of the crystals in Fig. 4(a) at different goniometer tilts. These patterns match well to the [101] and [212] zone axis patterns, respectively, for the γ-$Y_2Si_2O_7$ phase. Also, the calculated angle between these poles of 28.9°, for the cell parameters given by Liddell and Thompson,[23] matches fairly well to the angle calculated from goniometer readings of 30.1°. Two other zone axis patterns were also recorded for this crystal corresponding to the [100] and [102] zone axes for γ-$Y_2Si_2O_7$. The angles between all these poles fit fairly well to those that would be expected for the γ-$Y_2Si_2O_7$ phase, with the largest deviation between the expected value and that calculated from goniometer readings being $<1.7°$.

Although there is some similarity between certain diffraction patterns of γ-$Y_2Si_2O_7$ and δ-$Y_2Si_2O_7$, neither the angles between poles nor the diffraction patterns of Fig. 4(b) and (c), were in accordance with the cell parameters for the δ-$Y_2Si_2O_7$ phase. Thus, the analysed crystal in Fig. 4(a) was unequivocally determined as having the γ-$Y_2Si_2O_7$ phase.

Fig. 5(a) shows the edge of another larger crystal in the sub-scalar region of the 3:2:2 material crystallised at 1100°C. This crystal was also shown by EDX to be $Y_2Si_2O_7$. Fig. 5(b) and (c) shows two SAD patterns that match well with the expected patterns for the [110] and [11$\bar{1}$] axes of the δ-$Y_2Si_2O_7$ phase. The angles between these poles as measured from goniometer readings was 29.6°, as compared to the calculated angle based on the quoted lattice parameters for this phase[23] of 29.3°. Another zone axis pattern was also gained for this crystal which matched well to the expected pattern for the [120] direction of this phase. Furthermore, the angles between this direction and the [110] and [11$\bar{1}$] directions were both consistent with the cell parameters for the δ-$Y_2Si_2O_7$ phase. This sequence of patterns

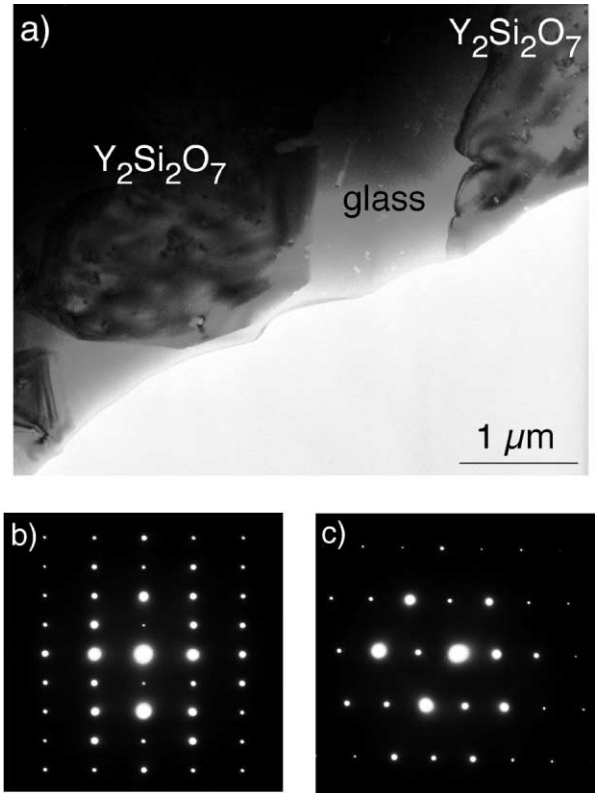

Fig. 4. TEM micrographs from an area with large $Y_2Si_2O_7$ crystals in the sub-scalar region of the 3:3:2 material heat-treated at 1100°C: (a) bright field image; (b) SAD pattern from one of the crystals matching [101] for γ-$Y_2Si_2O_7$; (c) SAD pattern from the same crystal matching [212] for γ-$Y_2Si_2O_7$.

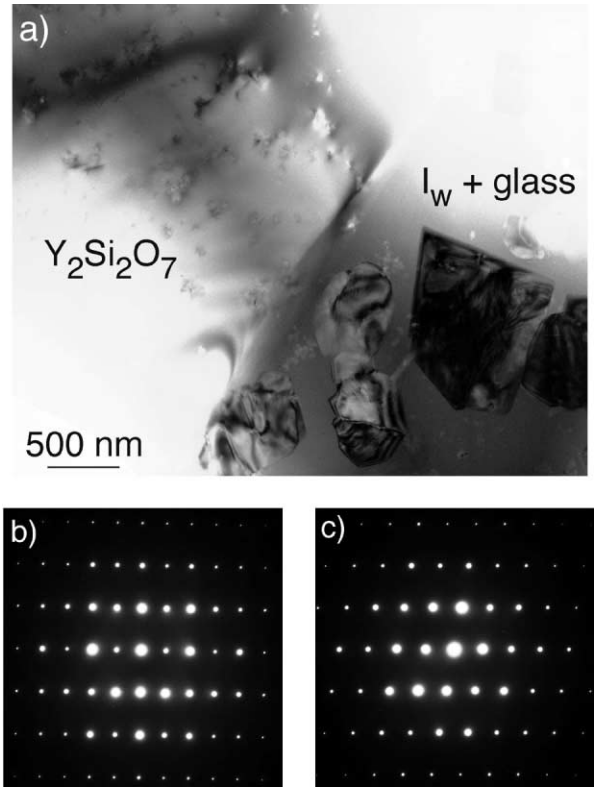

Fig. 5. TEM micrographs of another $Y_2Si_2O_7$ crystal in the sub-scalar region of the 3:3:2 material heat-treated at 1100°C (a) bright field image of the edge of a large $Y_2Si_2O_7$ crystal; (b) SAD pattern from this crystal matching [110] for δ-$Y_2Si_2O_7$; (c) SAD pattern from the same crystal matching [11$\bar{1}$] for δ-$Y_2Si_2O_7$.

could not match the γ-$Y_2Si_2O_7$ phase and this crystal can therefore be clearly identified as having the δ-$Y_2Si_2O_7$ structure.

Thus, crystals of both the γ and δ forms of $Y_2Si_2O_7$ could be identified as extending from the bottom of the oxide scale into the sub-scalar region of the 3:3:2 material crystallised at 1100°C. In some cases, there were large glass areas in close proximity to these $Y_2Si_2O_7$ crystals.

Large crystals of $Y_2Si_2O_7$ were also found in the thin foil specimen of the 3:3:2 material crystallised at 1200°C where the oxidation process seemed to have affected the whole material. One example of such a large crystal is shown in Fig. 6 as the large light coloured crystal that displays several bend contours and some planar faulting.

3.3. EDX and EELS analysis of I_w crystal and glass compositions

In an attempt to understand the cause of the significant grain coarsening in the sub-scalar region, the composition of crystals and glass in the two 3:3:2 thin foils from the specimen crystallised at 1100°C (see Fig. 2) were analysed using EDX to determine cation compositions and EELS to determine N contents from the N:O ratio. For each specimen, simultaneous EDX/EELS analyses were performed in 10–15 different areas for both the I_w crystals and the residual glass, to ensure that enough data were collected to reduce the chance of operator bias in the results.

An EEL spectrum of the energy region including the N K and O K edges is shown in Fig. 7, from a glass area in the unaffected bulk material with a relatively high N-content (≈13 anion %).

The composition of the I_w crystals showed no significant change from one thin foil to the other. In the case of the thin foil from the central region, the cation composition of the crystals was 46±1% Y, 37±2% Si, and 17±1% Al, with an anion composition of around 2±2% N, balance O. For the thin foil from the sub-scale region, the cation composition was 48±2% Y, 34±2% Si, and 18±1% Al, with an anion composition of 2±2% N, balance O. One interesting thing to note from this is that the N content of I_w phase is very low at around 2%; separate measurements on I_w crystals in another sample crystallised at 1150°C were also in accordance with this giving a N content of between 2 and 3 anion%.[24] This suggests that I_w is almost an oxide phase and is perhaps stabilised by just a small amount of nitrogen.

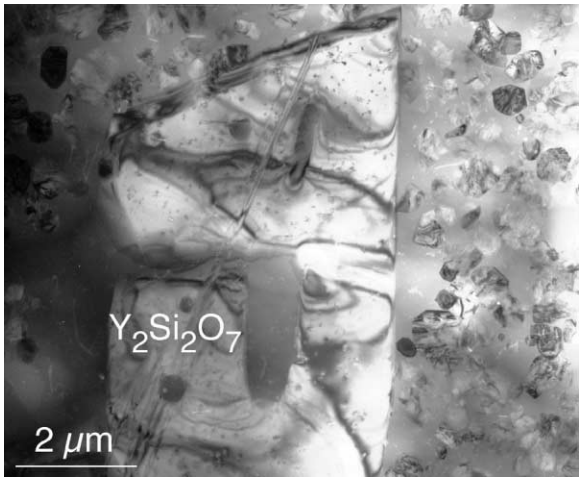

Fig. 6. Bright field image of a large $Y_2Si_2O_7$ crystal in the 3:3:2 material heat-treated at 1200°C.

When the residual glass was analysed in the two thin foils from the 3:3:2 specimen crystallised at 1100°C, however, a quite different story emerged. In the thin foil from the bulk, the glass was reasonably homogeneous with a cation content of 26±2% Y, 42±3% Si, and 33±2% Al (i.e. similar to previous results for residual glass in I_w glass-ceramics[11]). This is shown in Fig. 8(a), which is a graph of the Al, Y, and N contents plotted against the Si content for 15 different glass areas. The average nitrogen-oxygen content was calculated to be 8±5 anion% N, balance O. It is suspected that this N content may be a little underestimated as some areas seemed very beam damaged after analysis, and showed lower N contents on reanalysis.

In the thin foil from the sub-scalar region, however, the composition of the glass was rather less uniform. The average cation composition was 29±4% Y, 39±3% Si, and 32±2% Al. This figure includes some compositions close to those in the unaffected bulk material, together with a couple that were rich in Y and poor in Si as compared to that composition. The most extreme case was a composition for one large glassy area of 38% Y, 34% Si, 28% Al. This wider range of cation compositions can be clearly seen in Fig. 8(b), which is a graph of the Al, Y, and N contents against the Si content for several different glass areas in this specimen [plotted on the same axes as Fig. 8(a)].

This variability in cation content went together with a large variability in the N content. The average content was 5±4 anion%, which does not, in itself, represent a significant drop compared with the glass in the bulk. This average value includes, however, some areas with relatively high N contents (>8 anion%), as well as several others with very low N contents (<4 anion%). In particular, large areas of glass (many having a similar appearance to that in Fig. 4) tended to have very low nitrogen contents and sometimes had a noticeable Y excess and Si deficiency, with variable Al contents. In the graph of Fig. 8(b), the nitrogen contents for points that were definitely part of larger glass areas are marked with hollow triangles, and it can be seen that most of these had low N contents, although the two higher N contents (5.9 and 13%) were from the different parts of the same large glass area, which seemed to have a rather Si-

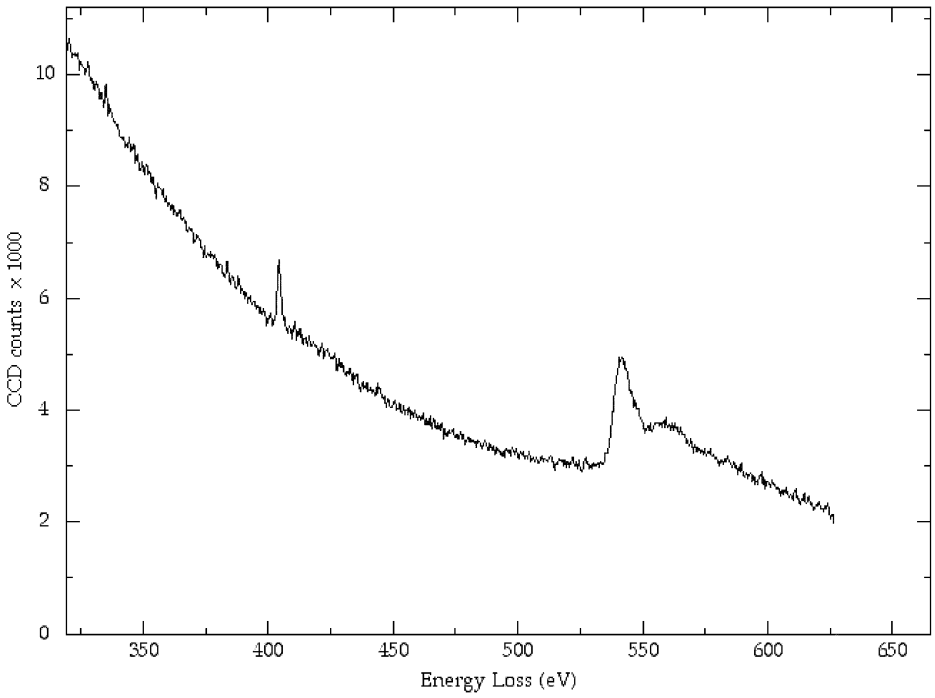

Fig. 7. An EEL spectrum of the energy region including the N and O edges from a glass area with a relatively high N-content (≈13 anion%) from the unoxidised central region of the 3:3:2 material heat treated at 1100°C.

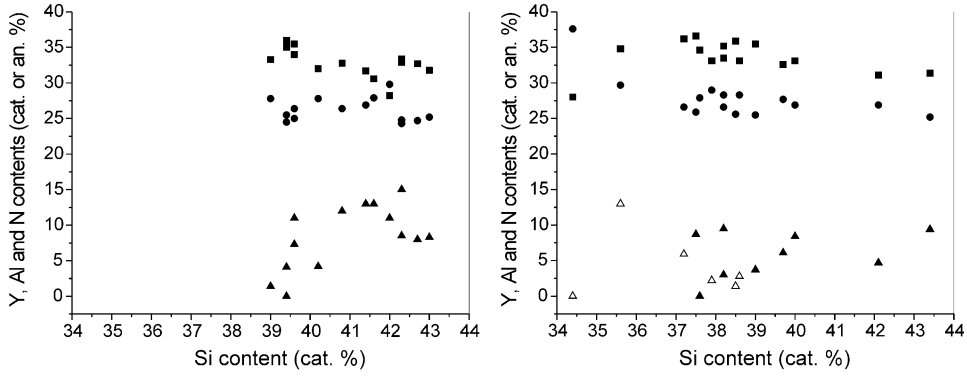

Fig. 8. Graphs of Y (circles), Al (squares), and N (triangles) content against Si content for residual glass areas in: (a) the oxidation unaffected bulk; (b) the sub-scalar region, open triangles denote N-content measurements for large glass areas.

depleted composition. In contrast to this, smaller areas of glass enclosed between I_w crystals displayed similar cation and anion compositions to the areas observed in the sample from the unaffected central region.

4. Discussion

At the temperatures of crystallisation, the residual glass is well above its T_g (which is probably less than 1000°C,[2,25] even if the change of its composition from the initial glass composition is considered), and thus there will be significant softening of the glass that would promote diffusion processes. This is quite similar to the situation in liquid phase sintered silicon nitrides where previous studies have shown that the resulting residual glassy intergranular phase is softened at elevated temperatures and is strongly implicated in the oxidation of such materials[6,8,9] with diffusion of various elements (especially O and cations originating from the sintering additives) being a significant part of this process.[6–9,26,27]

It is clear that the glass in the more open areas of the microstructure in the sub-scalar region of the 3:2:2 specimen was indeed affected by diffusion during crystallisation at 1100°C, as N contents are lower than is normal for the residual glass, and O is correspondingly enriched. Two different diffusion processes could account for the observed decrease in the N/O ratio. As observed for different types of liquid phase sintered silicon nitride ceramics and oxynitride glasses there would be an inward diffusion of O through the oxide scale down to the oxidation reaction site and the sub-scalar regions.[1,7,27]

Also, an outward transport of N would, in addition to the N released by the oxidation reaction, promote the observed formation of pores in the outer parts of the oxide scale (A in Fig. 1). It may be noted that the authors are not aware of any studies that present direct evidence for the outward diffusion of N from the sub-scalar region during oxidation of SiAlONs, although it is quite possible that this occurs concurrently with the inward diffusion of O.[6]

In addition to the anion transport, diffusion of the cation species is also occurring, especially in larger glass areas resulting in cation ratios that are often significantly changed with respect to the standard residual glass composition (often Y or Al enriched). This may well be part of the process that results in the formation and growth of large $Y_2Si_2O_7$ crystals, especially as large glass areas were sometimes observed adjacent to these $Y_2Si_2O_7$ crystals.

It may be objected that the crystallisation of I_w was not complete in the subscalar region when the inward diffusion of oxygen started to affect the microstructure but this is unlikely to have had a large effect for several reasons. Firstly, the crystallisation of the I_w phase at $\geqslant 1100^\circ C$ is thought to be relatively fast. Studies of crystallisation of the related B-phase at 1040°C showed that crystallisation is relatively rapid and is close to complete within 2 h.[18] Furthermore, on heating at normal heating rates (2–20°C min^{-1}), it was found that crystallisation was complete by the time that the furnace temperature had reached ≈1106°C.[18] Thus, crystallisation of B-phase glass compositions will be completed within minutes at temperatures of ≈1100°C. It is likely, therefore, that the crystallisation of the related I_w phase at ≈1100°C will be similarly rapid, so it is reasonable to assume that crystallisation will be complete in less than 1 h. On the contrary, the diffusion processes leading to the changes in residual glass composition that were noted are likely to be slower, happening over a period of several hours.

Secondly, measurements of the residual glass content in the sub-scalar region and the bulk show that to within experimental error the glass content is the same. This suggests that the microstructure in the sub-scalar region was already substantially crystallised before the glass composition was altered by diffusion, since an altered starting glass composition would probably yield a different crystalline fraction.

Finally, the inhomogeneity of the sub-scalar region, where glass areas mostly surrounded by I_w crystals have a composition indistinguishable from that of the residual glass in the bulk, whereas more open areas of glass have compositions affected by diffusion, suggests that the area originally had a microstructure and chemistry similar to the bulk prior to being affected by diffusion.

As has been shown previously, growth of I_w crystals in these materials mainly occurs through rotation and coalescence of crystals, which often results in the formation of orientational domain boundaries.[17] One result of forming a N-poor residual glass will be that the glass viscosity will be significantly reduced. This will then allow the movement and coalescence of I_w crystals to happen more freely than was possible in a more viscous glass having a higher N content. For this reason, the coalescence rate would be expected to increase leading to the formation of larger, heavily faulted, I_w crystals in sub-scalar and partially oxidised microstructures, as observed in the present investigation.

In the light of the above points, the difference in microstructure of the bulk of the 3:3:2 and 3.45:3:2 materials crystallised at 1200°C for 10 h may now be understood more clearly. The 3:3:2 materials have a significantly higher residual glass content than the 3.45:3:2 materials (about 35 and 25% respectively).[11] Since the diffusion that occurs below the oxide scale is restricted to the residual glass, then it is not surprising that the higher glass content 3:3:2 material is much more affected throughout the bulk by the oxidation than the 3.45:3:2 material. It may be noted that a specimen of 3:3:2 composition heat treated at this temperature for a longer time (50 h) was completely fractured after crystallisation,[11] presumably due to extensive oxidation throughout the sample. Thus, it may also be suggested that the oxidation resistance of the lower glass content 3.45:3:2 materials should, in general, be better than that of 3:3:2 materials, both because there will be less residual glass to transport oxygen into the sub-scalar regions, and because such MSiAlON glasses tends to be more susceptible to oxidation than MSiAlON crystalline phases.[4,10]

Finally, we note that the γ and δ forms of $Y_2Si_2O_7$ were those which could be identified by TEM observations in the outer sub-scalar regions of the specimen crystallised at 1100°C. This is mostly consistent with XRD data, which found different yttrium silicates (mainly γ and β forms) and aluminium silicate ($Al_2Si_4O_{10}$) present in the oxide scale on similar glass-ceramic materials.[28] This is also in accord with previous observations that these three forms of yttrium disilicate are the most frequently observed polymorphs in Y–Si–Al–O–N materials.[29,30–32] In contrast to this, the α, β, and γ forms are the most commonly observed polymorphs in yttrium disilicate prepared from oxide precursors, with the δ form sometimes observed after treatment at very high temperatures ($>1535^\circ C$).[23,30,33–35] The reasons for this can just be speculated at, but it may be possible that the presence of a very small concentration of N or Al in the $Y_2Si_2O_7$ formed by oxidation of Y–Si–Al–O–Ns could be implicated in this change of relative stability of the different polymorphs.

5. Conclusions

The microstructure of areas of I_w Y–Si–Al–O–N glass–ceramics which were affected by diffusion processes

occurring because of surface oxidation during crystallisation heat treatment have been compared with microstructures which were apparently unaffected by the oxidation process. It was found that the subscalar regions were characterised by a glass-ceramic microstructure with the I_w crystals having an anomalously large size, and the presence of some $Y_2Si_2O_7$ crystals. Both the γ and δ forms of $Y_2Si_2O_7$ were observed.

Combined EELS and EDX analysis revealed that the composition of the I_w crystals was mostly unaffected by the diffusion processes occurring in the sub-scalar regions during oxidation, and that they had a low nitrogen content of $\sim$2 anion%, but that the residual glass in the sub-scalar regions is affected with a significantly increased O/N ratio in some areas. The change in glass composition was found to be fairly inhomogeneous with more open areas of glass being more strongly affected than those surrounded by I_w crystals. The cation composition was also more scattered than in the oxidation unaffected bulk of the material, and in particular, some areas showed significantly increased Y and/or Al contents. It is thus clear that diffusion processes occur in the residual glass in the sub-scalar region.

It was proposed that the inward diffusion of O, possibly combined with a loss of N, in the glass would lead to a lowering of the viscosity which would allow the I_w crystals more freedom to move and coalesce, thus accounting for the increased size of the crystals in the subscalar areas.

It can, therefore, be concluded that oxidation is initiated by the inward diffusion of O into the residual glass with a concomitant effect of increasing the grain size of the I_w phase, coupled with a diffusion process leading to the formation of yttrium disilicate crystals which consumes the O-enriched / N-depleted residual glass.

Acknowledgements

We gratefully acknowledge the provision of financial support for this work from the European Commission under the TMR Research Networks scheme, grant number: FMRX- CT96- 0038 (DG 12- ORGS). Professor P Goursat is gratefully acknowledged for providing valuable comments on the manuscript. The other partners in the TMR NeoCeram network, Professors D.P. Thompson, J.-L. Besson, R.K. Harris, F. Cambier, and J.-C. Descamps, are thanked for their encouragement and for useful discussions.

References

1. Leng-Ward, G. and Lewis, M. H., In *Glasses and Glass Ceramics*, ed. M. H. Lewis. Chapman and Hall, London, 1989, Chapter 4, pp. 136–137.
2. O'Meara, C., Dunlop, G. L. and Pompe, R., Formation, crystallisation and oxidation of selected glasses in the Y–Si–Al–O–N system. *J. Eur. Ceram. Soc.*, 1991, **8**, 161–170.
3. Sebaï, M., Sjöberg, J., Goursat, P., Nestor, E., Flynn, R., Ramesh, R. and Hampshire, S., Oxidation behaviour of yttrium and neodymium oxynitride glasses. *J. Eur. Ceram. Soc.*, 1995, **15**, 1015–1024.
4. Sebaï, M., Penot, C., Goursat, P., Liddell, K., Thompson, D. P., Nestor, E., Ramesh, R. and Hampshire, S., Oxidation resistance of Nd–Si–Al–O–N glasses and glass-ceramics. *J. Eur. Ceram. Soc.*, 1998, **18**, 169–182.
5. Tulliani, J.M., Audoin, L. and Goursat, P., submitted to *J. Eur. Ceram. Soc.*
6. Clarke, D. R. and Lange, F. F., Oxidation of Si_3N_4 alloys: relation to phase equilibria in the system Si_3N_4–SiO_2–MgO. *J. Am. Ceram. Soc.*, 1980, **63**, 589–593.
7. McDonough, W. J., Wu, C.Cm. and Morgan, P. E. D., Internal phase changes in dense Si_3N_4 associated with high-temperature oxidation. *J. Am. Ceram. Soc.*, 1981, **64**, C45–C47.
8. Lewis, M. H. and Barnard, P., Oxidation mechanisms in Si–Al–O–N ceramics. *J. Mater. Sci.*, 1980, **15**, 443–448.
9. Persson, J., Ekström, T., Käll, P.-O. and Nygren, M., Oxidation behaviour and mechanical properties of β- and mixed α-β sialons sintered with additions of Y_2O_3 and Nd_2O_3. *J. Eur. Ceram. Soc.*, 1993, **11**, 363–373.
10. Tulliani, J. M., Goursat, P., Menke, Y., Hampshire, S. and Falk, L. K. L., unpublished work, 1999.
11. MacLaren, I., Falk, L. K. L, Díaz, A. and Hampshire, S., Preparation and characterisation of I_w-phase Y- and Er-Si–Al–O–N glass ceramics. *J. Am. Ceram. Soc.*, in press.
12. Rae, A. W. J. M., Yttrium silicon oxynitrides. PhD thesis, University of Newcastle upon Tyne, UK, 1976.
13. Gonon, M. F., Descamps, J.-C., Cambier, F. and Thompson, D. P., Determination and refinement of the crystal structure of M_2SiAlO_5N "B-phase" (M = Y, Er, Yb). *Ceram. Int.*, 2000, **26**, 105–111.
14. Liddell, K., Mandal, H. and Thompson, D. P., X-ray data for new Y–Si–Al–O–N glass geramics. *J. Eur. Ceram. Soc.*, 1997, **17**, 781.
15. Leng-Ward, G. and Lewis, M. H., Crystallisation in Y–Si–Al–O–N glasses. *Mater. Sci. Eng.*, 1985, **71**, 101–111.
16. Leng-Ward, G. and Lewis, M. H. In: Glasses, Glass Ceramics Chapter 4. ed. M. H. Lewis. Chapman Hall, London, 1989, pp. 138–142.
17. MacLaren, I., Falk, L. K. L, Díaz, A. and Hampshire, S. The formation of domain boundaries in the I_w-phase of Y- and Er–Si–Al–O–N *Philos. Mag. A*, in press.
18. Besson, J.-L., Lemercier, H., Rouxel, T. and Trolliard, G., Yttrium sialon glasses: Nucleation and crystallization of $Y_{35}Si_{45}Al_{20}O_{83}N_{17}$. *J. Non-Crystalline Sol.*, 1997, **211**, 1–21.
19. Stadelmann, P. and Jouneau, P. H., EMS On line. available on the internet at http://cimesg1.epfl.ch/CIOL/ems.html, Ecole Polytechnique Fédérale de Lausanne, Switzerland, 1995–1998.
20. MacLaren, I., Trusty, P. A. and Ponton, C. B., A transmission electron microscope study of hydrothermally synthesised yttrium disilicate powders. *Acta Mater.*, 1999, **47**, 779–791.
21. Egerton, R. F., *Electron Energy — Loss Spectroscopy in the Electron Microscope*, 2nd edn. Plenum Press, New York, 1996, pp. 284–286.
22. Egerton, R. F., *Electron Energy-Loss Spectroscopy in the Electron Microscope*, 2nd edn. Plenum Press, New York, 1996, pp. 281–283.
23. Liddell, K. and Thompson, D. P., X-ray diffraction data for yttrium silicates. *Br. Ceram. Trans. J.*, 1986, **85**, 17–22.
24. MacLaren, I. and Falk, L. K. L., Internal progress report from the TMR NeoCeram project, November 1999.
25. Díaz, A. and Hampshire, S., manuscript in preparation.

26. Falk, L. K. L. and Engström, E. U., Elemental concentration profiles in an oxidized silicon nitride material. *J. Am. Ceram. Soc*., 1991, **74**, 2286–2292.
27. Falk, L. K. L. and Rundgren, K., Microstructure and short-term oxidation of hot-pressed $Si_3N_4/ZrO_2(+Y_2O_3)$ ceramics. *J. Am. Ceram. Soc*., 1992, **75**, 28–35.
28. Díaz, A. and Hampshire, S., unpublished work, 2000.
29. Rouxel, T. and Verdier, P., SiC particle reinforced oxynitride glass and glass–ceramic composites: crystallization and viscoplastic forming ranges. *Acta. Mater*., 1996, **44**, 2217–2225.
30. Lee, W. E., Drummond, C. H., Hilmas, G. E. and Kumar, S., Microstructural evolution in near-eutectic yttrium silicate compositions fabricated from a bulk melt and as an intergranular phase in silicon-nitride. *J. Am. Ceram. Soc*., 1990, **73**, 3575–3579.
31. Hampshire, S., Nestor, E., Flynn, R., Besson, J.-L., Rouxel, T., Lemercier, H., Goursat, P., Sebaï, M., Thompson, D. P. and Liddell, K., Yttrium oxynitride glasses: properties and potential for crystallisation to glass-ceramics. *J. Eur. Ceram. Soc*., 1994, **14**, 261–273.
32. Dinger, T. R., Rai, R. S. and Thomas, G., Crystallization behaviour of a glass in the Y_2O_3–SiO_2–AlN system. *J. Am. Ceram. Soc*., 1988, **71**, 236–244.
33. Ito, J. and Johnson, H, Synthesis and Study of yttrialite. *Am. Mineral*., 1968, **53**, 1940–1952.
34. Trusty, P. A., Chan, K. C. and Ponton, C. B., Synthesis of sinteractive single-phase microstructure yttrium disilicate precursor powder using hydrothermal processing. *J. Mater. Res*., 1998, **13**, 3135–3143.
35. Moya, J. S., Díaz, M., Serna, C. J. and Mello-Castanho, S., Formation of a nanocrystalline yttrium disilicate powder by an oxalate gel method. *J. Eur. Ceram. Soc*., 1998, **18**, 1381–1384.